Journal of Alloys and Compounds 509 (2011) 3293–3298

Contents lists available at ScienceDirect

Journal of Alloys and Compounds

journal homepage: www.elsevier.com/locate/jallcom

Microstructure evolution and mechanical properties of nanocrystalline FeAl obtained by mechanical alloying and cold consolidation

M. Mhadhbi [a], M. Khitouni [a,*], L. Escoda [b], J.J. Suñol [b], M. Dammak [a]

[a] Laboratoire de Chimie Inorganique, 99/UR/12-22, University of Sfax, B. P. 1171, Sfax 3000, Tunisia
[b] Dep. de Fisica, Universitat de Girona, Campus Montilivi, Girona 17071, Spain

ARTICLE INFO

Article history:
Received 8 July 2010
Received in revised form 4 October 2010
Accepted 6 October 2010
Available online 9 December 2010

Keywords:
Mechanical milling
X-ray diffraction
Microstructure
Intermetallic alloys
Nanostructured Fe(Al)

ABSTRACT

In the present study high energy mechanical milling followed by cold temperature pressing consolidation has been used to obtain bulk nanocrystalline FeAl alloy. Fully dense disks with homogenous microstructure were obtained and bulk material show grain size of 40 nm. Thermal stability of the bulk material is studied by XRD and DSC techniques. Subsequent annealing at a temperature up to 480 °C for 2 h of the consolidated samples enabled supersaturated Fe(Al) solid solution to precipitate out fine metastable Al_5Fe_2, $Al_{13}Fe_4$ and Fe_3Al intermetallic phases. Low temperature annealing is responsible for the relaxation of the disordered structure by removing defects initially introduced by severe plastic deformation. Microhardness shows an increase with grain size reduction, as expected from Hall–Petch relationship at least down to a grain size of 74 nm, then a decrease at smallest grain sizes. This could be an indication of some softening for finest nanocrystallites. The peak hardening for the bulk nanocrystalline FeAl is detected after isochronal ageing at 480 °C.

1. Introduction

FeAl intermetallics possesses advantageous properties, in particular a high strength at both room and elevated temperatures, high specific stiffness, an excellent corrosion resistance at elevated temperatures under oxidizing, carburizing and sulfidizing atmospheres, relatively high electrical resistivity and low thermal conductivity [1–4]. Recent studies have demonstrated the feasibility of fabricating FeAl intermetallics by powder metallurgy, including hot isostatic pressing (HIP) [5], extruding [6,7], hot forging or pressing [8,9], powder injection molding [10] and cold consolidation [11–14]. The FeAl powders used for powder metallurgy processes were prepared mostly by MA [5,9,11,14]. The formation of nanocrystalline structures is possible in the ball-milled FeAl powders, thus helping improve the ductility [6]. Consolidation of mechanically alloyed (MA) powders into bulk, full-density compacts preserving nanometric grain size, which is crucial for possible application of nanophase materials, is not easy to achieve. In fact, full consolidation of nanocrystalline or amorphous alloy powder during conventional extrusion or consolidation was achieved only at high temperatures. In many of these cases, the elaborated bulk materials contain phases and microstructures that are frequently different from the initial ones or from desired phase. Alternatively, cold consolidation by severe plastic deformation (SPD) techniques can produce bulk samples, without significant phase transformation [11,13,14].

The present paper deals with preparation of nanocrystalline bulk Fe–Al alloy by MA, cold consolidation and subsequent annealing. The different tempers of the nanocrystalline alloy were characterized by X-ray diffraction (XRD), scanning electron microscopy. The thermal stability of consolidated sample was studied by differential scanning calorimetry (DSC). In addition, mechanical property of the nanocrystalline alloy was evaluated by microhardness measurement.

2. Experimental data

Pure elements, Fe (99.9%) and Al (99.3%), with respectively 80–60 and 120–80 μm, powders were separately weighted and mixed to get the desired composition (Fe–40 at% Al). Mechanical alloying was carried out to 20 h in a vibrator mixed Mill (Fritsch P9) at room temperature, using agate vials and ball, so that contamination debris, if any, should not be soluble in the intermetallic powder. Moreover, to protect the powders against oxidation, argon was introduced into the vials. Milling proceeds with a constant speed of rotation automatically fixed. In order to avoid the increase of the temperature inside the vials, the milling process was interrupted each 10 min for 15 min.

Nanocrystalline FeAl powder produced by MA was consolidated at room temperature using a uniaxial hydraulic press at 5 and 7 GPa for 5 min into cylindrical pellets of 10 mm diameter. The density of the sample was measured using Archimede's method. The microstructures were carried out with a wide angle X-ray diffractometer using Cu Kα radiation ($\lambda = 0.15406$ nm). Scans were collected over a 2θ range of 30–90° with a step of 0.02°. Microstructural parameters were calculated, from XRD data, by using Halder–Wagner method [15]. The instrumental broadening was determined using Si standard and subtracted from the experimental breadth to

* Corresponding author.
E-mail address: khitouni@yahoo.fr (M. Khitouni).

0925-8388/$ – see front matter © 2010 Elsevier B.V. All rights reserved.
doi:10.1016/j.jallcom.2010.10.214

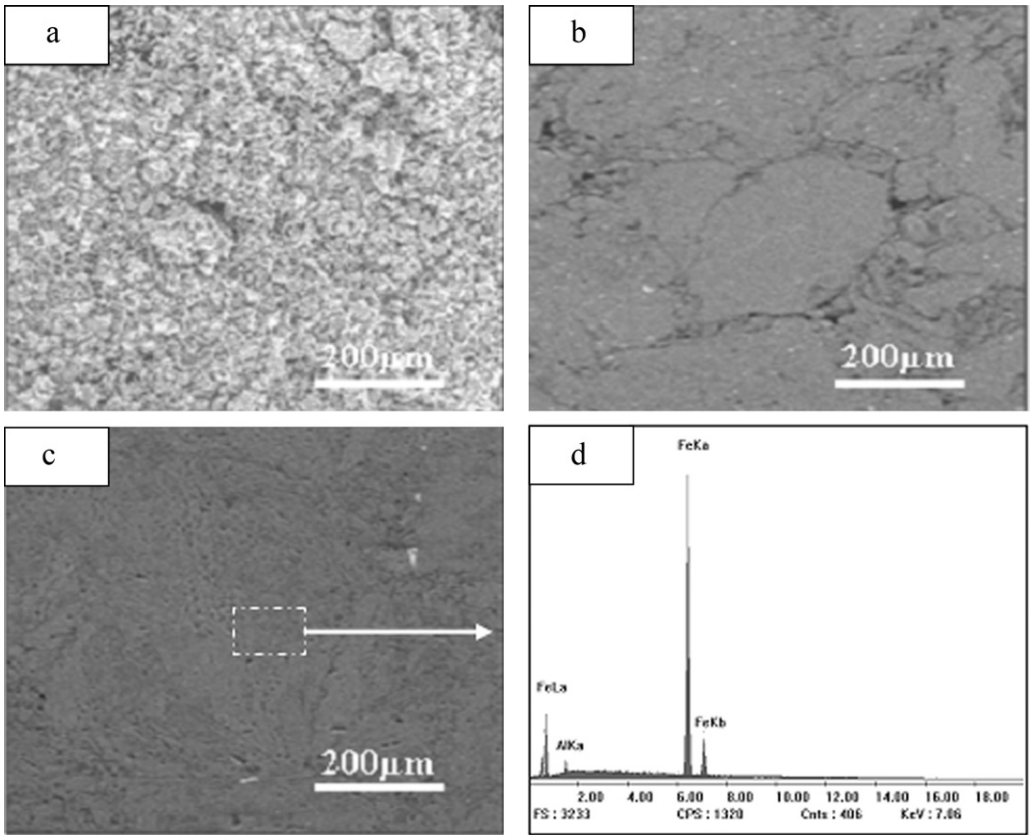

Fig. 1. SEM images of prepared Fe(Al) solid solution: (a) milled for 20 h, (b) consolidated under a stress of 5 GPa, (c) consolidated under a stress of 7 GPa and (d) the EDX analysis corresponding to (c).

obtain the physical broadening of each diffraction line. For the phase analysis, X'Pert High Score plus program was used.

The morphology and composition study was followed by scanning electron microscopy (SEM). Thermal behaviour was performed under Ar atmosphere using differential scanning calorimetry (DSC) at a temperature range from 35 to 700 °C and at a constant rate of 20 °C/min.

Mechanical hardness tests were performed on the consolidated and heated samples by using a METKON P005811 hardness tester. For each sample, the overall average hardness was obtained by using a 100 gf load indenter over random regions in five points.

3. Results and discussion

3.1. Microstructure of consolidated nanocrystalline Fe(Al) powder

The room temperature consolidation is chosen as a compaction process in the present work in order to retain the nanocrystalline structure obtained by mechanical milling. The conditions were established after many consolidation trials cited in recent work [11]. In the present work, the MA product after 20 h milling time was subjected to room temperature consolidation under stresses of 5 and 7 GPa. Typical SEM micrographs of the utilized powder and the consolidated samples are given in Fig. 1. During milling for 20 h, the fine powder tends to form a matrix of randomly welded thin layers of highly deformed particles (Fig. 1(a)). Fig. 1(b) corresponds to the consolidated milled powder under stresses of 5 GPa and shows an almost perfect regions. The prior particle boundaries are still visible and some pores are observed in the triple junctions of prior particle boundaries. This illustrates that the bonding of powder particles is not extremely good. The relative density, evaluated by the Archimedes method, is about 90%. However, the consolidated disk under stress of 7 GPa exhibits a fully dense microstructure without

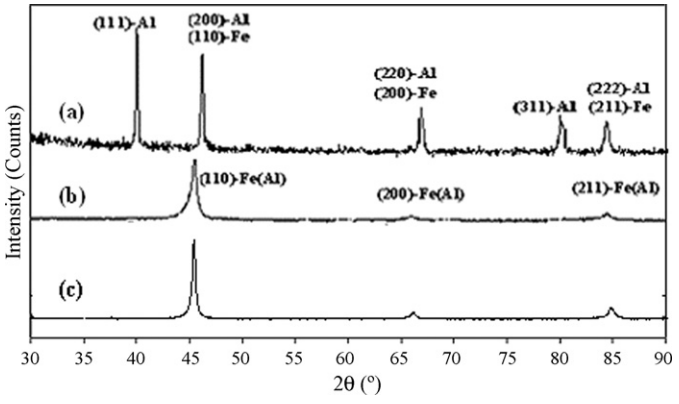

Fig. 2. XRD patterns of FeAl alloy: (a) before milling, (b) after milling and (c) after consolidation under a stress of 7 GPa.

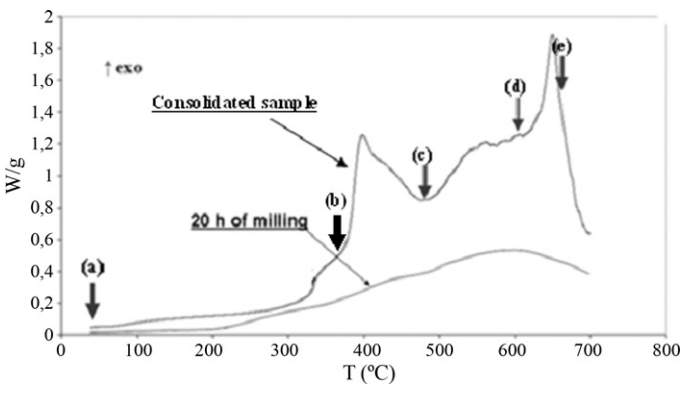

Fig. 3. DSC traces of the powder produced after milling for 20 h and consolidated under 7 GPa.

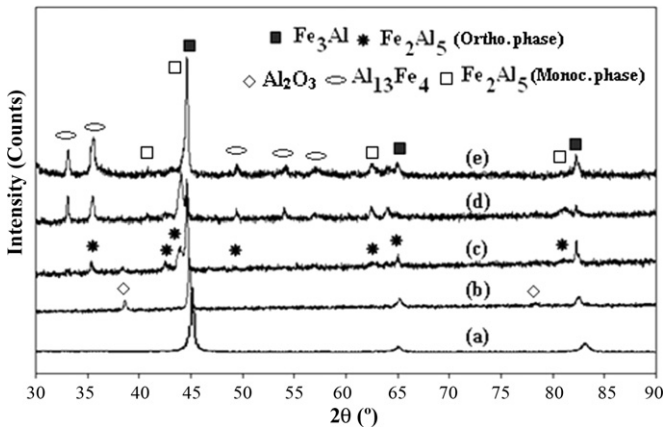

Fig. 4. X-ray diffraction patterns of consolidated Fe(Al) powder: (a) after consolidation under a stress of 7 GPa, (b) after heating at 370 °C, (c) after heating at 480 °C, (d) after heating at 610 °C and (e) after heating at 660 °C.

any distinct porosity and the prior particle boundaries Fig. 1(c). For that, the relative density increased to about 98%. The EDX analysis of typical region in Fig. 1(c) shows the presence of Fe and Al elements (Fig. 1(d)).

The investigated samples were further characterized by XRD, and main results are represented in Fig. 2. Fig. 2(a) and (b) shows typical X-ray diffraction patterns of FeAl powder before and after milling for 20 h. With further milling, the most intense Al line (1 1 1) disappears completely, which indicates that all the Al atoms are dissolved in the bcc Fe lattice to form the Fe(Al) solid solution. The details of this experimental step have been described elsewhere [16]. Fig. 2(c) shows the XRD pattern of the consolidated Fe(Al) powder under a stress of 7 GPa. Comparing the diffractogram of bulk Fe(Al) sample with the one of the powder before consolidation, one can see that there is no change in the constituent phase presents in the powder after consolidation and all peaks became a little sharper than those in the patterns of the milled powder before consolidation. This little reduction in peaks width indicates the occurrence of grain growth and/or internal strain release. The estimated mean crystallite sizes and the mean lattice strain of the Fe(Al) alloy are given in Table 1. The maximum variations of the crystallite size and the lattice strain are $\Delta D \approx 31$ nm and $\Delta\varepsilon \approx 0.75\%$, respectively.

During the consolidation process the sample was high-pressed under some GPa, thus high strain imposed for certain size. However, the increase of the mean crystallite size in the consolidated sample can indicates that high strain imposed by severe plastic deformation causes partial crystallization of the nanostructure. The same effect of consolidation already observed during severe plastic deformation of gas atomised $Al_{90}Fe_5Nd_5$ [13] and of mechanical milled Al–4.5wt%Cu [11], and $Al_{90}Fe_7Zr_3$ [17] alloys. Another feature in these XRD patterns is that all the peaks are shifted to higher values of angles in the case of consolidated sample. This is due to the decrease of the lattice parameter during compaction process. The maximum variation was $\Delta a \approx -0.0022$ Å. This decrease is probably explained by the presence of compressive stress fields within the nonequilibrium grain boundaries inside of crystallite [18]. Lattice strain caused by SPD is commonly attributed to the generation and movement of dislocation [11,19]. So, for MA samples subjected to SPD, dislocations are considered as the main defects. The calculated values of dislocation densities, ρ_D, of the MA and consolidated Fe(Al) samples are about 2.9×10^{16} and $1.27 \times 10^{16}/m^2$, respectively. This decrease can explain the partial dynamic recrystallization of the original deformed structure from the milled powder to the consolidated one. Usually, in conventional polycrystalline materials, the grain boundaries GBs are thought to be barriers to the dislocations motion, therefore the slight decrease in the dislocations density within consolidation process indicates a softening of the GBs. When the GBs have turned soft or relaxed, the amount of the dislocations piled up near the GBs will be decreased. McQueen et al. [20–23] have also carefully studied the dynamic recrystallization behaviour in cold deformed materials. They found that strain hardening combinations are outweighed by the opportunities for annihilation and array polygonization in the restorative mechanism of dynamic recovery. On the other hand, the passage of grain boundaries (GB) through the metal alters the progress of deformation lowering stress by replacing regions of high dislocation density from strain hardening reactions, with soft regions ripe for the operation of dislocation sources. This process called discontinuous dynamic recrystallization is dependent on nucleation; it is found primarily in low stacking fault energy (SFE) metals, such as Cu, Ni and γ-Fe alloys above $0.5T_M$ (melting K) due to the low level of dynamic recovery [24–26].

3.2. Thermal stability of consolidated nanocrystalline Fe(Al) powder

Fig. 3 shows DSC traces of Fe(Al) samples (MA for 20 h and consolidated under stress of 7 GPa). As shown, the DSC trace of 20 h milled powder exhibited overlapping exothermic peaks. The details of this DSC experimental step have been described elsewhere [27]. These overlapping exothermic peaks became more clearly as fourth peaks, in the case of consolidated powder. The first exothermic peak was rather small and its onset and peak temperatures were approximately 322 and 371 °C, respectively. The second exothermic peak became stronger, and its onset and peak temperatures were

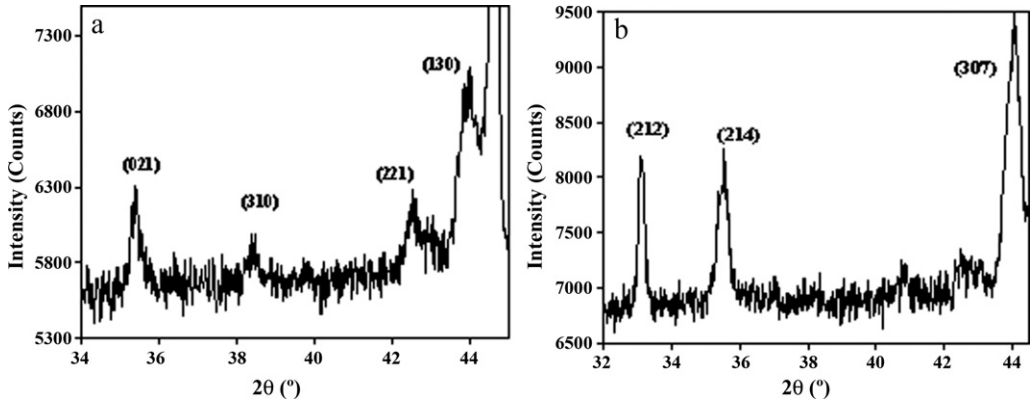

Fig. 5. Reflections of (a) Al_5Fe_2 and (b) $Al_{13}Fe_4$ phases used for the calculation of their mean values of crystallite and lattice strains.

Table 1
Evolution of structure in the investigated FeAl alloy after MA, consolidation and annealing at deferent temperatures.

Processes types	Phases formed	Structure	<D> (nm)	ε (%)
MA for 20 h	FeAl	bcc	10	1.85
MA + consolidated	FeAl + Al_2O_3	Bcc/Romb	41/. . .	1.10/. . .
MA + consolidated + heated at 370 °C	FeAl + Al_2O_3	bcc/ortho	68/35	0.7/0.4
MA + consolidated + heated at 480 °C	FeAl + Fe_2Al_5	bcc/ortho	74/65	0.65/0.35
MA + consolidated + heated at 610 °C	FeAl + Fe_2Al_5 + $Al_{13}Fe_4$	bcc/monoc/ortho	80/65/45	0.5/0.25/0.15
MA + consolidated + heated at 660 °C	Fe_3Al + Fe_2Al_5 + $Al_{13}Fe_4$	bcc/monoc/ortho	92/—/86	0.15/. . ./0.05

approximately 371 and 480 °C, respectively. The third exothermic peak was rather small and large and its onset and peak temperatures were approximately 484 and 610 °C, respectively. The fourth exothermic peak became stronger, and its onset and peak temperatures were approximately 610 and 700 °C, respectively.

In order to understand the phase transformations corresponding to each of the exothermic peaks shown on the DSC trace, XRD analysis was performed on the samples produced by heating the as consolidated sample to temperatures above different exothermic peaks, as shown by the arrows in Fig. 3. The obtained XRD patterns are shown in Fig. 4(b)–(e), respectively. As shown in Fig. 4(b), there is a small amount of Al_2O_3 (Space group R-3c; a = 4.7180 Å, b = 4.7180 Å and c = 12.8180 Å [28]) formed after heat-treated consolidated powder at 370 °C. The formation of Al_2O_3 is associated with the oxygen that is absorbed at the powder surface when exposed to air after ball milling. Comparing the diffractogram of annealed sample at 370 °C (Fig. 4(b)) with the one obtained after room temperature consolidation (Fig. 4(a)), one can see that, except the formation of fine Al_2O_3, there is no change in the constituent phases present in the case of material obtained after consolidation. In addition, all peaks became a more little sharper than those in the patterns of the consolidated sample. This little reduction in peaks width is probably explained by a partial remove of the structural defects. Thus the first exothermic peak in the DSC trace (Fig. 3) of consolidated sample is attributed to the structure relaxation of the disordered structure of Fe(Al) solid solution by mechanisms of atomic-scale interchange and the movement of defect (e.g. dislocations with APBs). Annealing at 480 °C enabled supersaturated Fe(Al) solid solution to precipitate out Al_5Fe_2 intermetallic (space group: Cmcm; a = 7.6486 Å, b = 6.4131 Å and c = 4.2165 Å [29]) (Fig. 4(c)). According to the Fe–Al phase equilibrium diagram [30], for the Fe concentration of 60 at% there is

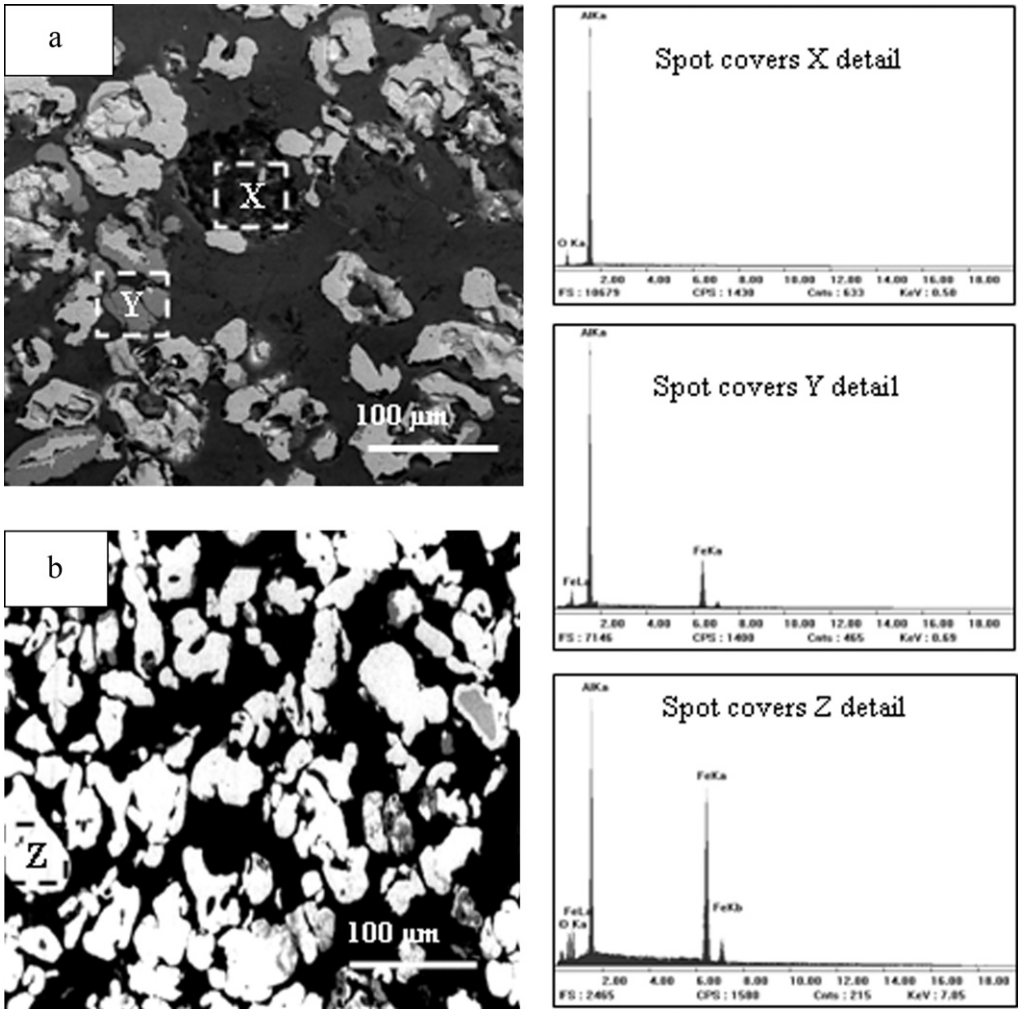

Fig. 6. SEM images of consolidated Fe(Al) powder: (a) after heating at 480 °C, (a) after heating at 660 °C.

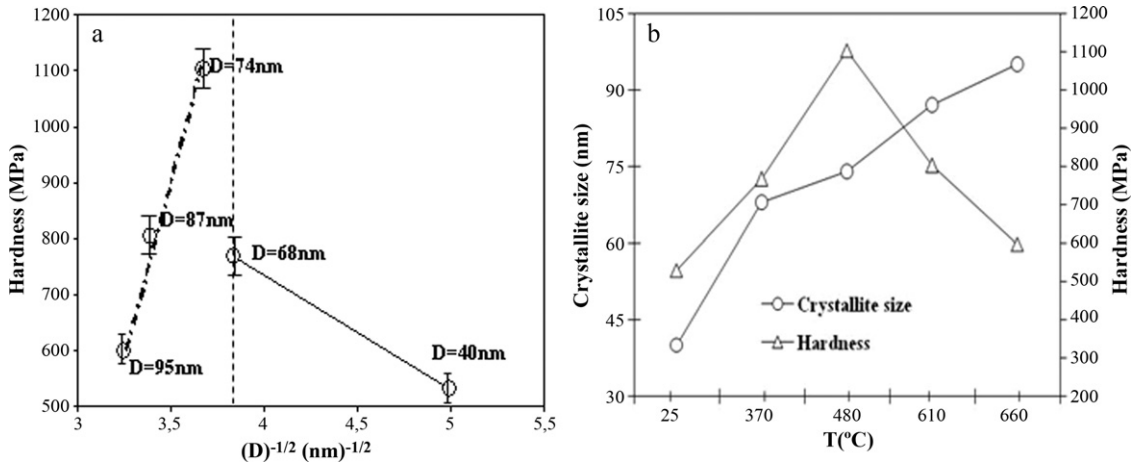

Fig. 7. (a) Variation of microhardness as a function of square root of the grain size to test the Hall–Petch relationship for the Fe(Al) consolidated samples, (b) variation of hardness and grain sizes of consolidated samples as a function of annealing temperatures, showing the peak hardening after isochronal ageing at 480 °C.

a two-phase FeAl + Fe_3Al field. However, mechanical alloying is a non-equilibrium processing technique, thus the phase composition and transformation of its products can differs from those predicted using phase equilibrium diagrams. For example, one can see that annealing of consolidate Fe(Al) solid solution at 480 °C resulted in starting precipitation of fine metastable Al_5Fe_2 intermetallic from the supersaturated Fe(Al) solid solution. The reason for preferred formation of metastable Al_5Fe_2 intermetallic can be attributed to the nonequilibrium nature of MA and also to the lower enthalpy of formation of Al_5Fe_2 ($\Delta H_f = -22$ kJ/mol) in comparison to that of other intermetallics [31]. The nucleation of the Al_5Fe_2 intermetallic at temperature range [370–480 °C] can explain the existence of the second exothermic peak in the DSC trace (Fig. 3) of consolidated sample. In the case of annealing at 610 °C, an $Al_{13}Fe_4$ intermetallic (space group: Bmmm; $a = 7.7510$ Å, $b = 4.0336$ Å and $c = 23.7710$ Å [32]) appears in the existing of Al_5Fe_2 intermetallic (Monoclinique $a = 9.9100$ Å, $b = 10.8110$ Å and $c = 8.8240$ Å [33]), which was manifested by sharpening of diffraction peaks, and of the partially ordered Fe_3Al intermetallic (Fig. 4(d)). Thus the third exothermic peak in the DSC trace (Fig. 3) is attributed to the appearance of these intermetallic phases. Annealing at 660 °C resulted in formation of ordered Fe_3Al intermetallic (space group: Fm3m $a = 5.800$ Å [34]) (appears in the existing Al_5Fe_2 and $Al_{13}Fe_4$ phases) (Fig. 4(e)). This can explain the appearance of the fourth exothermic peak in the DSC trace (Fig. 3). In addition, this peak can probably contain of the recrystallization and to the grain growth phenomena occurred in the FeAl intermetallics.

Besides the signs of phase changes, another feature in the bulk materials XRD patterns is that all the peaks become a little sharper while increasing the annealing temperature. This reduction in peaks width is due to the increase of the mean crystallite size and the decrease of the mean lattice strain. The estimated mean crystallite sizes for the phases in the compacted and heated samples (where it was reasonable) are given in Table 1. The mean values of crystallite size and lattice strain for the metastable Al_5Fe_2 and $Al_{13}Fe_4$ intermetallics were calculated by using the (0 2 1), (3 1 0), (2 2 1) and (1 3 0) and (2 1 2), (2 1 4) and (3 0 7) peaks represented in Fig. 5, respectively. One can see a limited growth of grain size took place during heating of consolidated samples and the nanoscale grain size has been retained after consolidation process followed by heating.

Fig. 6(a) and (b) shows the SEM images of the heated consolidated samples at 480 and 660 °C for 2 h, respectively, and the corresponding EDX. The obtained microstructures exhibit microparticles with particle sizes ~60 μm. From the EDX analysis, the black particles correspond to Al rich phases (Fig. 6(a), Y zone) whereas the white ones represent the iron-rich zones (Fig. 6(a), Z zone). Comparing these results with those presented in Fig. 4(c) and (e), we can attribute the black and the white particles to the Fe_2Al_5 and Fe_3Al, respectively.

3.3. Mechanical properties of consolidated nanocrystalline Fe(Al) powder

Microhardness was adopted to evaluate the mechanical properties of the nanocomposite Fe(Al) alloy obtained after consolidating the powder milled for 20 h, under a stress of 7 GPa at room temperature. Fig. 7(a) shows the variation of microhardness as a function of reciprocal square root of the grain size in compacted Fe(Al). The hardness increases linearly with the reciprocal square root of the grain size up to a grain size of about 74 nm. Hall–Petch behaviour is thus demonstrated over the range of grain sizes from 95 nm to 74 nm, with the Hall–Petch slope describing the grain size sensitivity having a similar value to that found for conventional grain sizes. This behaviour is believed to be associated with perfect densification and interparticle bonding at these small grain sizes which are found in the materials compacted in room temperature then heated at lower temperatures. However, it is interesting to note that when the crystallite sizes drops below 74 nm, the slope of the plot becomes negative. The microhardness falls at the smallest grain sizes that this could be an indication of some softening for finest nanocrystallites (the inverse H–P relationship [35–37]). Moreover, other studies have, alternatively, considered that hardness may fall at very small grain sizes, for example as it becomes impossible to accommodate the several dislocations required to form pile-up at a grain boundary [19,38]. The variation of microhardness of the FeAl samples, obtained after 2 h annealing at different temperatures, was plotted as a function of temperature of annealing (Fig. 7(b)). The microhardness increases with increase in annealing temperature up to 480 °C, while annealing at a higher temperatures of 610 and 660 °C resulted in sharp decrease in microhardness. Based on these observations, one can conclude that 480 °C is the peak of hardening for the nanocrystalline FeAl obtained after 20 h MA and cold consolidation. The high hardness values of 1.1 GPa can be probably attribued to the effects of nanocrystalline Al_5Fe_2 and $Al_{13}Fe_4$ phases formed at this annealing temperature (Fig. 4(c)) and high defect density incorporated during MA of the investigated alloy. Furthermore, the decrease of the hardness values, at higher temperatures, is expected due to the increase in volume fraction of soft nanocrystalline phases and to the grain coarsening of FeAl phases

and annihilation of defects being created during MA. Moreover, it is interesting to mention here that even though the hardness of nanocomposite of FeAl alloy drops after annealing at 660 °C, it is still higher than that of hardness of cold compacts of FeAl alloy.

4. Conclusion

Room temperature consolidation of nanocrystalline Fe(Al) solid solution prepared by MA after 20 h has been attempted by high pressure under stress of 7 GPa. Microstructural analysis after process of consolidation and after annealing allowed the following features to be remarked:

(i) Almost full consolidation of the MA powder occurred after 7 GPa where the consolidated material had a nanocrystalline structure with grain size of 40 nm.
(ii) Compared to MA powder, high strain imposed on the fine particles by consolidation causes partial crystallization of the nanostructure.
(iii) Heating of the consolidated samples resulted in formation of nanocrystalline Fe_2Al_5 and $Al_{13}Fe_4$, and Fe_3Al intermetallic phases and finer grain size may be retained.
(iv) Mechanical property measured in microhardness testing shows strengthening down to a grain size of 74 nm and Hall–Petch behaviour is thus demonstrated over the range of grain sizes from 95 to 74 nm. At the smallest grain sizes, the microhardness falls indicating of some softening for finest nanocrystallites. The peak hardening for the nanocrystalline FeAl obtained after 20 h MA and cold cnsolidation is detected after isochronal ageing at 480 °C.

Acknowledgement

Financial support from MICYT MAT2006-13925-C02-02 (FEDER) project is acknowledged.

References

[1] N.S. Stoloff, Mater. Sci. Eng. A258 (1998) 1–14.
[2] P.F. Tortorelli, J.H. DeVan, Mater. Sci. Eng. A153 (1992) 573–577.
[3] S.C. Deevi, V.K. Sikka, C.T. Liu, Prog. Mater Sci. 42 (1997) 177–192.
[4] S.C. Deevi, V.K. Sikka, Intermetallics 4 (1996) 357–375.
[5] H. Skoglund, M.K. Wedel, B. Karlson, Intermetallics 12 (7–9) (2004) 977–983.
[6] D.G. Morris, S. Gunther, Mater. Sci. Eng. A 208 (1) (1996) 7–19.
[7] J. Chao, D.G. Morris, M.A. Munoz-Morris, J.L. Gonzalez-Carrasco, Intermetallics 9 (4) (2001) 299–308.
[8] M.A. Munoz-Morris, A. Dodge, D.G. Morris, Nanostruct. Mater. 11 (7) (1999) 873–885.
[9] M. Kransnowski, T. Kulik, J. Alloys Compd. 495 (2010) 382–385.
[10] K. Kato, T. Masui, J. Jpn. Soc. Powder Powder Metall. 49 (9) (2002) 787–792.
[11] M. Azabou, M. Khitouni, A. Kolsi, Mater. Charact. 60 (2009) 499–505.
[12] R. Birringer, Mater. Sci. Eng. A117 (1989) 33–43.
[13] A.R. Yavari, W.J. Botta Filho, C.A.D. Rodrigues, C. Cardoso, R.Z. Valiev, Scr. Mater. 46 (2002) 711–716.
[14] G. Ji, D. Goran, F. Bernard, T. Grosdidier, E. Gaffet, Z.A. Munir, J. Alloys Compd. 420 (2006) 158–164.
[15] J.I. Langford, R. Delhez, Th. H. de Keijser, E.J. Mittemeijer, J. Appl. Crystallogr. 41 (1988) 173.
[16] M. Mhadhbi, M. Khitouni, L. Escoda, J.J. Suñol, Mater. Lett. 64 (2010) 1802–1805.
[17] W.J. Botta Filho, J.B. Fogagnolo, C.A.D. Rodrigues, C.S. Kiminami, C. Bolfarini, A.R. Yavari, Mater Sci. Eng. A 375–377 (2004) 936–941.
[18] K. Zhang, I.V. Alexandrov, K. Lu, Nanostruct. Mater. 9 (1997) 347–350.
[19] F.A. Mohamed, Acta Mater. 51 (14) (2003) 4107–4119.
[20] H.J. McQueen, E. Evangelista, Czech. J. Phys. B38 (1988) 359–372.
[21] H.J. McQueen, in: M. Tiryakioglu (Ed.), Advances in Metallurgy of Aluminum Alloys (J.T. Staley Symposium), ASM International, Materials Park, OH, 2001, pp. 351–360.
[22] H.J. McQueen, C.A. Imbert, J. Alloys Compd. 378 (2004) 35–43.
[23] R.D. Doherty, D.A. Hughes, F.J. Humphreys, J.J. Jonas, D. Juul-Jensen, M.E. Kassner, W.E. King, T.R. McNelley, H.J. McQueen, A.D. Rollett, Mater. Sci. Eng. 238 (1998) 219–274.
[24] H.J. McQueen, in: S. Yue, E. Essadiqi (Eds.), Thermomechanical Processing of Steel (Jonas Symposium), Met. Soc. CIM, Montreal, 2000, pp. 323–333.
[25] H.J. McQueen, N.D. Ryan, in: S.V. Raj (Ed.), Rate Processes in Plastic Deformation II, TMS-AIME, 2000, Mater. Sci. Eng. A322 (2002) 43–63.
[26] T. Sakai, J.J. Jonas, Acta Metall. 32 (1984) 189–209.
[27] G. Ji, T. Grosdidier, H.L. Liao, J.P. Morniroli, C. Coddet, Intermetallics 13 (2005) 596.
[28] G. Ji, J.P. Morniroli, T. Grosdidier, Scr. Mater. 18 (2003) 1599.
[29] A.J. Bradley, A.H. Jay, Proc. R. Soc. Lond., Ser. A A13 (1932) 210.
[30] L.W. Finger, R.M. Hazen, J. Appl. Phys. 49 (1978) 5823.
[31] M. Ellner, J. Mayer, Scr. Metall. Mater. 26 (1992) 501.
[32] O. Kubaschewski, Iron Binary Phase Diagrams, Springer-Verlag, Berlin, 1982, p. 5–9.
[33] Y. Zou, S. Saji, K. Kusabiraki, MRS Res. Bull. 37 (2002) 123.
[34] M. Ellner, Acta Crystallogr. Sec. B: Struct. Sci. 51 (1995) 31.
[35] A.S. Ilyushin, W.E. Wallace, J. Solid State Chem. 17 (1976) 385.
[36] C. Suryanarayana, Int. Mater. Rev. 40 (1995) 42–64.
[37] C.E. Carlton, P.J. Ferreira, Acta Mater. 55 (2007) 3749.
[38] H. Conrad, J. Narayan, Scr. Mater. 42 (2000).